The Role of ARID1A in the Nonestrogenic Modulation of IGF-1 Signaling

Sham Jdeed[1], Edina Erdős[2], Bálint L. Bálint[2], and Iván P. Uray[1]

ABSTRACT

Gaining pharmacologic access to the potential of ARID1A, a tumor suppressor protein, to mediate transcriptional control over cancer gene expression is an unresolved challenge. Retinoid X receptor ligands are pleiotropic, incompletely understood tools that regulate breast epithelial cell proliferation and differentiation. We found that low-dose bexarotene (Bex) combined with the nonselective beta-blocker carvedilol (Carv) reduces proliferation of MCF10DCIS.com cells and markedly suppresses ARID1A levels. Similarly, Carv synergized with Bex in MCF-7 cells to suppress cell growth. Chromatin immunoprecipitation sequencing analysis revealed that under nonestrogenic conditions Bex + Carv alters the concerted genomic distribution of the chromatin remodeler ARID1A and acetylated histone H3K27, at sites related to insulin-like growth factor (IGF) signaling. Several distinct sites of ARID1A enrichment were identified in the *IGF-1* receptor and *IRS1* genes,

associated with a suppression of both proteins. The knock-down of ARID1A increased IGF-1R levels, prevented IGF-1R and IRS1 suppression upon Bex + Carv, and stimulated proliferation. *In vitro* IGF-1 receptor neutralizing antibody suppressed cell growth, while elevated IGF-1R or IRS1 expression was associated with poor survival of patients with ER-negative breast cancer. Our study demonstrates direct impact of ARID1A redistribution on the expression and growth regulation of IGF-1–related genes, induced by repurposed clinical drugs under nonestrogenic conditions.

Implications: This study underscores the possibility of the pharmacologic modulation of the ARID1A factor to downregulate protumorigenic IGF-1 activity in patients with postmenopausal breast cancer undergoing aromatase inhibitor treatment.

Introduction

Most successful therapies aiming for controlling breast cancer target the estrogen receptor alpha (ER) or the receptor tyrosine kinase Her2 (1). However, at least 20% of all breast cancers are not dependent on these two drivers of tumor growth, and others acquire drug resistance through various mechanisms during the course of treatment (2). These patients have fewer options for effective targeted therapies. In the preventive setting, hormone receptor status of the premalignant breast epithelium offers little predictive power, as the majority of all samples contain ER, but expression is restricted to a minority of the cells (3). Thus, new ER-independent targets with antitumor potential are in the forefront of interest.

Retinoid X receptor (RXR) activation occurs without the involvement of steroid nuclear receptors. Although RXRs are promiscuous in their activation profile regarding the selection of partner receptors, they are also highly selective in their ligand preference at pharmacologic dosing (4). RXR-selective retinoids (rexinoids) elicit receptor-specific responses at nanomolar concentrations (5). Nevertheless, long-term efforts to limit side-effects led to the identification of

synergistic interactions at subclinical doses between rexinoids and other clinical drugs (6–8). In this study, we utilized the synergy between the sole FDA-approved rexinoid bexarotene (Targretin, LGD1069; abbreviated here as Bex) and the nonselective beta-adrenergic antagonist, Carv, to enhance Bex's antiproliferative activity and elucidate associated genomic events only indirectly controlled by the activated nuclear receptors.

To identify new, RXR-induced genomic mechanisms that exert control over key mitogenic pathways, we profiled proteomic responses in ER-negative, noncommitted ductal carcinoma *in situ* (DCIS) cells. This screen identified the AT-Rich Interaction Domain 1A (ARID1A) as the most prominent change upon Bex + Carv treatment. ARID1A is a tumor suppressor that is frequently mutated in different types of cancers and is critical in controlling cellular immortality and mutability (9, 10). Patients with breast cancer with high ARID1A protein expression levels have better overall survival compared with patients with lower ARID1A levels (11). Molecularly, the ARID1A protein is a standard member of the multisubunit SWI/SNF (BAF) chromatin remodeling complex that plays an important role in the maintenance of genome stability (12). As part of the DNA damage response, some of the SWI/SNF functions are presumed to safeguard against cell transformation and carcinogenesis (13). However, the mechanisms by which ARID1A regulates transcription and growth through chromatin regulation are largely unclear.

The MCF10DCIS.COM is an ER-negative cell line and a model with similarities to human DCIS lesions *in vivo*. These cells retain "bipotent" progenitor qualities, able to form both basal-like DCIS and develop into luminal-type cells (14). In contrast, MCF-7 cells have been used as a classic model of estrogen-responsive breast cancer, in which estrogen withdrawal abrogates mitogenic signaling (15). The genomic behavior of ARID1A in response to estrogenic cues has been extensively studied in MCF-7. Xu and colleagues demonstrated that by binding chromatin at *cis*-regulatory elements of ER, ARID1A takes on a key role in the therapeutic response of ER-positive breast cancer and in the maintenance of a luminal phenotype (16). While this connection

[1]Department of Clinical Oncology, Faculty of Medicine, University of Debrecen, Debrecen, Hungary. [2]Department of Biochemistry and Molecular Biology, Faculty of Medicine, University of Debrecen, Debrecen, Hungary.

Corresponding Author: Iván Uray, Department of Clinical Oncology, Faculty of Medicine, University of Debrecen, Nagyerdei krt. 98., Debrecen 4032, Hungary

justifies the impact of the SWI/SNF (BAF) chromatin-regulatory complex on the prognosis of ER-positive breast cancers, the correlation of ARID1A with response to chemotherapy and outcome in triple-negative breast cancers (TNBC) points to an estrogen receptor–independent role of ARID1A (17). Therefore, we hypothesized that ARID1A, in addition to modulating ER-dependent growth, must play a role in growth regulation through alternative mechanisms. To identify such mechanisms we used the previously characterized luminal breast cancer model MCF-7 under estrogen deprivation and studied the distribution of ARID1A and the associated changes in the activation of chromatin regions relevant for cell proliferation.

We show that Bex + Carv treatment of MCF-7 cells results in increased binding of ARID1A at several genomic locations of growth regulatory genes, and reduced proliferation under nonestrogenic conditions. ARID1A binding regulates the expression of two members of the insulin-like growth factor (IGF)-axis, insulin-like growth factor-1 receptor (IGF-1R), and insulin receptor substrate 1 (IRS1), through novel enhancer sites. Our data suggest a repressive role of ARID1A in regulating the IGF-1 axis and consequently cell proliferation.

Materials and Methods

Cell culture and treatment

MCF10DCIS.com and MCF-7 cells with confirmed identity were kindly provided by Powel H. Brown (UT MD Anderson Cancer Center, Houston, TX) and used within 6 passages after thawing. Cells were periodically tested for *Mycoplasma*-free condition using the Promokine PCR-based assay, but no more than 3 months before use. Cell lines were authenticated by deep sequencing at the time of the study. DCIS cells were maintained in DMEM/F12 medium supplemented with 10% horse serum and 5 mmol/L glutamine. MCF-7 breast cancer cells were cultured in DMEM (Biosera, catalog no. MS00ER1003), supplemented with 10% FBS (Biosera, catalog no. S00402000M) and streptomycin/ampicillin/glutamine (Corning, catalog no. 30–0090CI). Cells were maintained in a humidified atmosphere with 5% CO_2 at 37°C. Twenty-four hours prior to treatment with agents of interest, media were changed to phenol-red free DMEM (Gibco, catalog no. A14430–01) to exclude estrogen-like effects. Cells were seeded in 12-well plates for protein and RNA isolation or in 20-cm plates for chromatin immunoprecipitation (ChIP), and treated at 70% confluence in triplicate.

Bex (Targretin, LGD1069; Bex) and Carv were purchased from MedChemExpress and Sigma, respectively. The drugs were dissolved in DMSO/ethanol (50/50) solution, which was used as a control treatment (Vehicle). The agents were diluted in cell culture media before adding to cells, with DMSO final concentration not to exceed 0.01%.

Protein quantification by reverse-phase protein arrays

MCF10DCIS.com cell extracts were prepared for reverse-phase protein arrays (RPPA) experiments as described previously (18). In short, a minimum of 10^5 cells per sample replicate washed twice with PBS and lysed in ice-cold HEPES lysis buffer (pH 7.4, containing 1% Triton X-100, 1 mmol/L EGTA, 1.5 mmol/L $MgCl_2$, 150 mmol/L NaCl, 100 mmol/L NaF, 10 mmol/L sodium pyrophosphate, 1 mmol/L Na_3VO_4, 10% glycerol) and supplemented with proteinase inhibitors (Roche Applied Science). All consecutive steps were carried out by the RPPA core facility at the MD Anderson Cancer Center (Houston, TX) including antibody probing by validated antibodies (tcpaportal.org/mclp), signal detection,

data processing and normalization, as adapted for the TCGA patient samples platform.

Reverse transcription-quantitative polymerase chain reaction

Total RNA was isolated using TRIzol reagent (Thermo Fisher Scientific). One microliter total RNA was used to produce cDNA using RevertAid reverse transcriptase (Thermo Fisher). Quantitative real-time PCR was carried out using TaqMan assays with the following conditions: initial denaturation at 95°C for 2 minutes followed by 40 cycles of denaturation at 95°C for 10 seconds then annealing and extension at 60°C for 30 seconds for each cycle. Absolute quantification method was used for data analysis. mRNA expression levels of each gene of interest were normalized to corresponding β-actin levels in that sample. Sequences of the qPCR oligos used are shown in Supplementary Table S3.

ChIP

20 million cells or 5 million cells were used for each IP for ChIP sequencing (ChIP-seq) or ChIP-qPCR, respectively. Cells were cross-linked in 1% methanol-free ultrapure formaldehyde for 10 minutes at room temperature, followed by addition of 1 mol/L glycine to quench formaldehyde autofluorescence. Cells were washed twice with ice-cold PBS then lysed by ChIP lysis buffer (1% Triton X-100, 0.1% SDS, 150 mmol/L NaCl, 1 mmol/L EDTA pH = 8.0, 20 mmol/L Tris pH = 8.0) with protease inhibitor cocktail tablets (Roche, cOmplete Mini, catalog no. 11836153001) added. Cell nuclei pellet was collected by centrifugation at 4°C with 12,000 × g for 1 minute and washed three times with ChIP lysis buffer. To fragment and shear chromatin, cell lysates were sonicated (3×5 minute cycles with 30 seconds on and 30 seconds off) using a Bioruptor Plus sonicator. The input sample was set aside as 10% of the sheared chromatin from each IP. Magnetic beads were used for immunoprecipitation by preparing a 1:1 mixture of protein A and protein G beads (catalog no. 10002D and 10004D, Thermo Fisher Scientific), blocked overnight with freshly prepared and filtered 0.5% BSA in PBS, and 190 μL or 50 μL beads were used for each IP in case of 20 million cells or 5 million cells, respectively. The sheared chromatin lysate was diluted in ChIP lysis buffer (1:9). To reduce the background signal generated from nonspecific interactions, the diluted sheared chromatin was incubated with beads coated with nonspecific IgG antibody overnight at 4°C. During the clearing step a mixture of protein A and protein G beads (after blocking) was incubated with an antibody against the protein of interest, either ARID1A (PSG3X, Santa Cruz Biotechnology, sc-32761x), acetyl-Histone H3 (K27, Cell Signaling Technology, 8173 s), or nonspecific IgG antibody, for overnight incubation at 4°C.

Sheared and cleared chromatin was incubated with beads coated with antibodies overnight at 4°C. The beads–antibody–protein–DNA complex was washed four times using ChIP washing buffers. To elute protein–DNA complexes, the beads were incubated with elution buffer (0.1 mol/L NaHCO3, 1%SDS) for 15 minutes at 1,000 rpm at room temperature. Input samples were included in the process starting from the elution step. To de-crosslink protein–DNA interactions, samples were incubated with 0.2 mol/L NaCl overnight at 65°C. Afterwards, DNA was purified by the addition of 10 μg RNase A (10 μg/μL), 20 μg proteinase K (20 μg/μL), 0.04 mol/L Tris-HCl pH = 7.0, 0.02 mol/L EDTA pH = 8.0, the mixture was incubated for 2 hours at 45°C on a thermomixer at 1,000 rpm. The last purification step was performed using MinElute PCR purification kit (catalog no. 28004, Qiagen) for ChIP samples to be sequenced or with High Pure PCR Template Preparation Roche Kit in case of ChIP-qPCR. DNA concentration

measured by the Qubit dsDNA HS assay. Library preparations and sequencing of ChIP samples were performed by the Genomic core facility (University of Debrecen, Debrecen, Hungary). Enrichment of specific target regions in DNA samples were tested in qPCR reactions.

ChIP-qPCR

ARID1A-binding events and H3K27ac marks identified in ChIP-seq were validated through ChIP-qPCR. IP and input samples were diluted 3-fold with nuclease-free water after DNA purification. Input samples were used as control; the amount of DNA from each IP sample was normalized to its corresponding input sample. One microliter DNA from each sample was used in qPCR reaction using SYBR Green I Master (Roche Diagnostics GmbH) as a fluorescence reporter. Primer sequences against ARID1A-binding regions used for ChIP-qPCR are shown in Supplementary Table S4.

ChIP-seq data processing

Fastq files (75 bp single-end reads) were obtained from the Genomic core facility, University of Debrecen. ChIP-seq data were analyzed by a published computational pipeline (19). Raw data were aligned to an hg19 reference dataset using Burrows–Wheeler Aligner (BWA). Peaks were called using HMCan (20). Artifact peak list was downloaded from the Encyclopedia of DNA Elements (ENCODE) and was removed from our peak sets. Overlap regions were determined using Bedtools with intersectBed command. Reads were normalized to sequencing depth through bam-coverage function and bigwig files were generated to visualize binding events with the Integrative Genomics Viewer (IGV).

Motif enrichment analyses were performed using Homer software with findMotifsGenome.pl command. The size parameter was 100 bp. Tag density values were calculated on the basis of summits of peaks flanking with $\pm 1,000$ base pair region for ARID1A and with $\pm 2,000$ for H3K27ac using Homer software with annotatePeaks.pl command options. Annotation was performed using Homer software with annotatePeaks.pl command. The sequencing data used in our manuscript are publicly available on NCBI's Sequence Read Archive (SRA) site under the sample Acc nos.: SRX13941915, SRX13941916, SRX13941917, SRX13941918, SRX13941919, SRX13941920, BioProject PRJNA799783.

Protein quantification by Western blotting

For Western blots cells were lysed in RIPA lysis buffer (150 mmol/L sodium chloride, 1.0% NP-40, 0.5% sodium deoxycholate, 0.1% SDS, 50 mmol/L Tris pH 8.0 plus protease inhibitor cocktail). Cell lysates were sonicated for 5 minutes (5 cycles, 30 seconds on, 30 seconds off) using a Bioruptor Plus sonicator (Diagenode S.S). Total protein concentration was measured using BCA assay. Denatured proteins (20–40 μg) were electrophoresed on 6% SDS-polyacrylamide gel, transferred to a PVDF and blocked with 5% low-fat milk in Tris-buffered saline (TBS) buffer for 1 hour (h) at room temperature (RT). Blots were probed with primary antibodies (see Supplementary Table S5) overnight at 4°C against ARID1A (1:1,000) and β-actin (1:5,000), followed by washing steps with TBS plus 0.1% Tween-20 (TBST) buffer. Membranes were incubated with anti-rabbit or anti-mouse Alexa Fluor (488 or 680 nm) conjugated secondary antibodies (1:30,000) for 1 hour at room temperature, followed by (5×5) washing steps with TBST. Blots were developed using an Odyssey CLx imaging system (LI-COR Biosciences). Western blot band signal intensity was quantitated using ImageJ software. The relative abundance of proteins of interest was calculated after normalization to β-actin levels as a housekeeping protein.

Immunocytochemistry/Immunofluorescence

Cells were seeded in 96-well optical plate, treated at 70% confluence, and fixed with 4% formaldehyde in PBS for 30 minutes at room temperature. Cells were washed three times with PBS then incubated with permeabilization solution (0.5% Triton X-100 in PBS) for 40 minutes at room temperature. To prevent nonspecific binding cells were incubated with blocking buffer (1% BSA/10% normal goat serum/ 0.3 mol/L glycine in 0.1% PBS-Tween) for 1 hour at room temperature, followed by washing steps with PBST three times. Primary antibody was added and incubated with the cells overnight at 4°C (Supplementary Table S5), followed by washing steps (3×5) with PBST. Secondary antibody (Alexa Fluor–conjugated antibodies 1:1,000) was added to cells and incubated for 1 hour at room temperature. The protein–primary Ab–secondary Ab complex was then cross-linked by incubating the cells with 4% formaldehyde in PBST for 10 minutes, followed by quenching using 100 mmol/L ammonium chloride for 10 minutes at room temperature. Cell nuclei were stained with DAPI (1 μg/mL) for 15 minutes at room temperature, followed by 3×5 minutes wash with PBST. Cells were imaged under an inverted fluorescent microscope (LEICA DMi8) using LasX software.

siRNA transfection

MCF-7 cells were seeded in a 24-well or 96-well optical plate. Transfection was conducted at 70% cell confluence. Transfection conditions were optimized to reach 70% to 80% knock-down efficiency using a pool of three ARID1A-specific siRNAs (TriFECTa RNAi Kit, Integrated DNA Technologies) at 10 nmol/L final concentration and Dharmafect 1 transfection reagent (DharmaFECT, DharmaCon, catalog no. T-2001–02). During the first 12 hours of transfection, cells were maintained in antibiotic-free reduced serum medium (OPTI-MEM, REF 31985–062). RNA or protein extracts were generated from the transfected cells to measure the knock-down levels through qRT-PCR or Western blotting, respectively.

Proliferation assay and image analysis

MCF-7 and MCF10DCIS.com cells were seeded in 96-well optical plates, and treated at 20% confluence with agents of interest. After 5 days (4 days in the case of MCF10DCIS.com) of treatment with Bex and/or Carv, cells were fixed with 4% formaldehyde in PBS for 30 minutes at room temperature. Cells were washed with PBS for 3×5 minutes then incubated with permeabilization solution (0.5% Triton X-100 in PBS) for 40 minutes at room temperature, followed by washing steps. Cell nuclei were stained with DAPI (1 μg/mL) for 15 minutes at room temperature, washed once with PBS and imaged across the total well surface using a fluorescent microscope (LEICA DMi8). Image analysis and cell counting based on nuclear segmentation of their DAPI signal was performed using ImageJ software. For cell-by-cell analyses, CellProfiler 4.1 (Broad Institute Inc.) was used. Cells were segmented by the nuclear label and cell outlines by cytoplasmic staining using minimum cross-entropy thresholding. To assess target protein levels a minimum of 200 cells per replicate were analyzed.

Colony formation assay (soft agar assay)

1 mL agarose (1%) was added to 1 mL 2× full DMEM, then 1.5 mL mixture was added to each well/6-well plate to form the bottom layer and left for 30 minutes at room temperature for solidification. To generate the top layer, 1 mL agarose (0.6%) was mixed with 1 mL 2× full DMEM and about 1.5×10^4 MCF-7 cells. Cells were kept at 37°C and 5% CO_2 for 4 weeks. Treatment containing medium was replaced every third day. Pictures for the colonies were taken using phase

contrast mode within LEICA DMi8 microscope using the LasX software. Colonies larger than 300 μm in diameter were counted using ImageJ. The experiment was performed in three biological replicates.

Neutralization of MCF-7 cells proliferation using anti–IGF-1R antibody

MCF-7 cells were seeded in 96-well optical plate and maintained in normal DMEM or phenol-red free DMEM. Cells were treated for 3 days with 11 μg/mL IGF-1R antibody (R&D Systems, MAB391). After that, cells were fixed with 4% formaldehyde in PBS 1× for 30 minutes at room temperature. Cells were washed with PBS (3×5) then incubated with permeabilization solution (0.5% Triton X-100 in PBS) for 40 minutes at room temperature, followed by washing steps. Cell nuclei were stained with DAPI (1 μg/mL) for 15 minutes at room temperature. All cells were counted by automated fluorescent microscopy (LEICA DMi8) using the LasX software based on DAPI signal, representing cell nuclei. Image analysis was performed using ImageJ software.

Survival analysis

Recurrence-free survival (RFS) of patients with breast cancer was assessed using the KMplotter (kmplot.com) software (21). Cohorts were split at median values, IGF-1R (Affymetrix probe 225330_at), and IRS1 (probe 242979_at) transcript levels were determined using the JetSet best probe set. Cases were stratified by ER-status – IHC and microarray-defined subtypes.

Statistical analysis

Three independent biological replicates were performed for each experiment. Power calculations were not performed. Statistical values are expressed as the mean ± SD. Comparisons between two groups were performed using the unpaired two-tailed Student t test. Comparisons between more than two groups were performed using one-way ANOVA test followed by Tukey *post hoc* test. $P < 0.05$ represents statistically significant difference between the studied groups.

Results

Identifying ARID1A as a putative actor in the cellular rexinoid response

To assess the growth-inhibitory effect of Bex and score its most effective combinations for synergy minimal dose–response matrices based on high-content microscopy assays were analyzed. The dose–response relationship of Bex and Carv over 4 days in MCF10DCIS.com cells confirmed the enhanced antiproliferative effect of the two compounds at concentrations greater than 100 nmol/L each (**Fig. 1A**). To identify mediators of this drug interaction, changes in the expression levels of 285 cancer-related proteins were quantified using RPPA. Rank order of the proteins that were significantly different (at $P < 0.001$) in response to Bex + Carv treatment relative to vehicle included 28 candidates (Supplementary Table S1). After applying a threshold of a 20% minimum change, 19 candidates remained, and only 9 of those changes were significantly ($P < 0.05$) different from the effect of Bex alone (**Fig. 1B**).

The expressions of five proteins changed in the same direction in response to the combination as to Bex alone, suggesting additive or synergistic effects and not an antagonistic interaction between Bex and Carv. Three of these candidates (PLK1, Stathmin-1, Cyclin-B1) are directly linked to cell-cycle regulation, while acetyl-CoA carboxylase

(ACC1) is a major regulator of lipogenesis. ARID1A, a tumor suppressor, was selected for further study based on the greatest effect size (>50%) detected and the highest level of significance ($P < 6 \times 10^{-05}$), and because of the less obvious connections to rexinoid-dependent cell growth regulation (**Fig. 1C**).

To determine whether these agents were also effective in ER-positive cells, MCF-7 luminal breast cancer cells were treated with Bex and Carv for 5 days. Although individually both Bex and Carv modestly suppressed growth, their combination exhibited markedly stronger inhibition of proliferation (**Fig. 1D**), compared with the effects of either drug alone. In contrast, anchorage-independent growth measured by colony formation assays (**Fig. 1E**) did not show a difference in response to this treatment.

Genomic changes and increased genomic occupancy of ARID1A after Bex + Carv treatment in MCF-7 cells

To study the genomic behavior of ARID1A under antiproliferative conditions, MCF-7 cells were cultured in phenol red-free media and in the presence of low-dose Bex and Carv for 48 hours, and rexinoid-induced changes in genome-wide occupancy by ARID1A were measured. Both experimental agents are devoid of primary estrogenic effects. Chromatin IPs coupled with massively parallel DNA sequencing (ChIP-seq) were performed to identify binding events associated with drug treatment. ChIP-seq dataset analysis showed that with either treatment, chromatin areas bound by ARID1A were located mainly in intergenic and intronic regions (**Fig. 2A**), suggesting that ARID1A is predominantly a *trans*-acting partner to the transcription complex, in the absence of estrogenic cues. The majority of all peaks of ARID1A occupancy irrespective of treatment, were located between 50 and 500 kb, either upstream or downstream of the TSSs (**Fig. 2B**), and less than 5% of all putative binding sites appeared in promoter or coding regions. The sequencing data indicated that 63% of ARID1A binding sites in the Bex + Carv–treated sample were unique and about 34% overlapped with vehicle-treated samples (**Fig. 2C**). Overall, 16,000 ARID1A binding events were detected in vehicle-treated samples and over 27,000 binding sites were detected after Bex + Carv treatment; only 10,000 sites were shared between the two treatments. Thus, far more binding events were gained than lost (over 17,000 vs. 6,000), in response to Bex + Carv (**Fig. 2C–E**). ARID1A has been shown to strongly colocalize with the K27-acetylated H3 histone protein (H3K27ac) during transcriptional activation at enhancer sites and prevent H3K27 hyperacetylation at active super-enhancers (22). Therefore, we used genomic binding of H3K27ac to mark transcriptionally active regions in chromatin and help interpret changes in ARID1A occupancy. In contrast to ARID1A enrichment in 63% of all binding events following Bex + Carv treatment, the newly occupied H3K27ac active marker sites adjacent to ARID1A represented only 9% (5,660 of the total 62,854) of all binding sites (**Fig. 2C–E**).

Motif enrichment analysis between ARID1A genomic occupancy and other transcriptional regulators demonstrated that ARID1A-bound sites were frequently enriched at gene loci involved in the regulation of cell proliferation and differentiation. These sites included Grainyhead Like Transcription Factor 2 (*GRHL2*), TRE (a motif for AP-1), and, most prominently, Forkhead Box M1 (*FOXM1*) motifs, occurring with both unchanged or altered ARID1A binding (**Fig. 2F**). While interactions of ARID1A with estrogen response elements (ERE) in MCF-7 cells treated with Bex + Carv were confirmed by the motif analysis, no retinoid response elements or half-sites were found among the ARID1A-binding motifs (Supplementary Table S2).
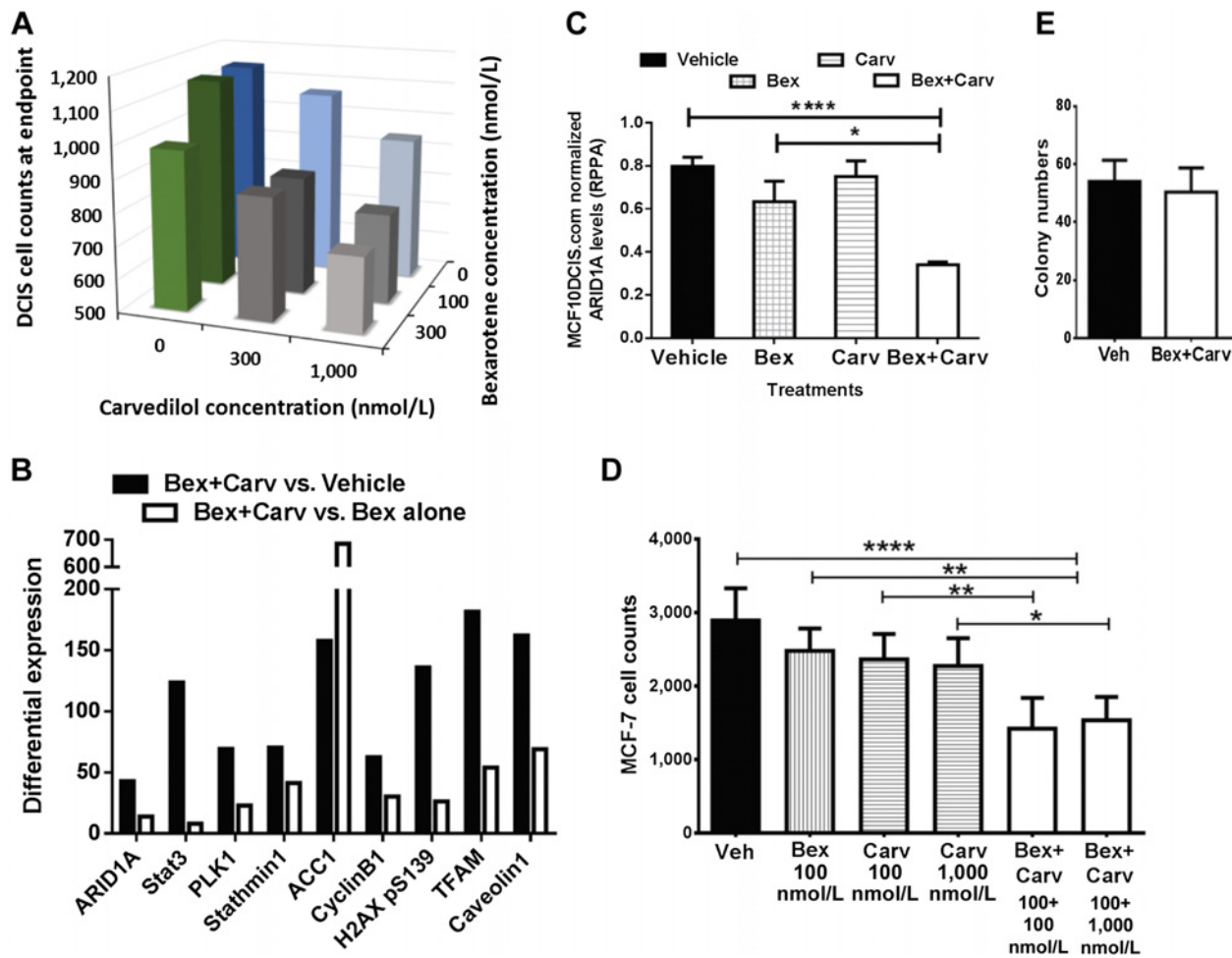
Figure 1.
Selection of ARID1A as a marker associated with breast cancer cell growth suppression by Bex combined with Carv. **A,** Dose–response profile of the effect of Bex and Carv on the proliferation of MCF10DCIS.com cells, measured by automated microscopic cell counting after 4 days of treatment. Distinct colors mark ranges of average cell counts per field of view (DAPI stained nuclei imaged at 5×). **B,** Comparison of differential protein expressions between low-dose (100 nmol/L) Bex + Carv versus Vehicle (dark bars) or Bex + Carv versus Bex alone (open bars), in significant changers of both categories, based on RPPA analysis of MCF10DCIS.com cell extracts. **C,** Comparison of ARID1A protein levels in DCIS cells treated with vehicle, 100 nmol/L Bex, 100 nmol/L Carv or their combination, based on RPPA measurements. **D,** MCF-7 cell counts evaluated by microscopy after 5 days of Bex and/or Carv treatment (Veh; Vehicle, Bex + Carv; DAPI-stained nuclei imaged at 5×). **E,** Colony formation assay of MCF-7 cells upon Bex + Carv or vehicle treatment, average colony counts from three replicates are shown. The results are expressed as mean ± SD. *, $P < 0.05$, **, $P < 0.01$, ****, $P < 0.0001$ by one-way ANOVA, Tukey *post hoc* test.

ARID1A mediates the regulation of IGF-1R and IRS1 by Bex + Carv in MCF-7 cells

To sort out genes that are relevant for the regulation of cell growth, increased ARID1A-binding events in response to Bex + Carv exposure of MCF-7 cells were clustered according to gene ontology (GO) categories of the affected genes. On the basis of the high-occupancy binding sites of specific motifs, GO analysis of the annotated genes illustrated that ARID1A-bound genes were significantly enriched in categories of mammary gland epithelial cell proliferation, mammary gland development, and the insulin-like growth factor (IGF) receptor signaling pathway upon Bex + Carv treatment, compared with controls (**Fig. 3A**). In dose escalation animal studies, higher doses of Bex caused significant reductions in IGF-1 levels (23). As IGF signaling is thought to play a significant role in the regulation of cell growth and differentiation, we conducted a more in-depth analysis of the ChIP-seq data for putative ARID1A-binding regions in IGF-related genes

by sequencing. To qualify as a candidate region, ARID1A peaks in every case coincided with a dip in H3K27ac occupancy. Our query identified enrichment in 4 distinct regulatory regions across the *IGF-1R* gene (+ 6 kb, +100 kb, +131 kb, or +211 kb from transcription start site (TSS); see diagram in **Fig. 3B**) and in three putative regulatory regions related to the *IRS1* gene (+ 643 kb, + 676 kb, or +684 kb from TSS; **Fig. 3C**).

ARID1A binding and enrichment to these regions of interest was validated by qPCR detection. Immunoprecipitation of chromatin by ARID1A antibodies recapitulated the sequencing results (**Fig. 3D** and **E**). Three of the 4 regions in the *IGF-1R* gene, those located 100 kb, 131 kb and 211 kb downstream from the transcription start site, were confirmed as significantly elevated in ARID1A binding by ChIP-qPCR (**Fig. 3D**). Two of 3 regions in the *IRS1* gene indicated a trend of increased ARID1A binding upon Bex + Carv, although failed to reach statistical significance (**Fig. 3E**). H3K27ac histone marks flanking each
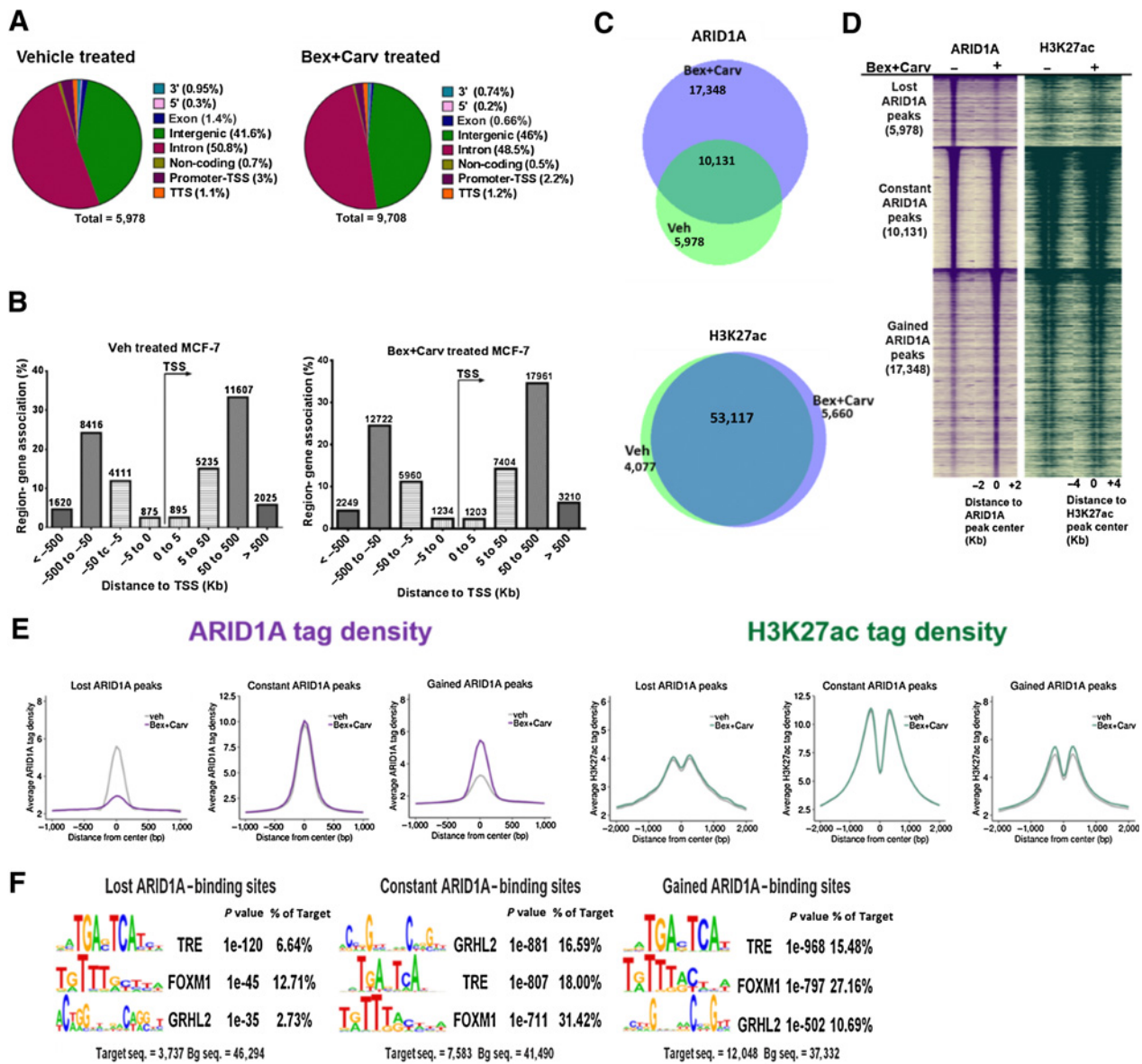
Figure 2.
Changes in the genomic distribution of ARID1A and H3K27ac in MCF-7 cells in response to the combination of Bex and Carv. **A,** ARID1A genomic distribution of ARID1A binding site localization in control and Bex + Carv–treated samples. **B,** Distribution of ARID1A occupancy in relation to transcription start sites (TSS) in vehicle and in Bex + Carv–treated samples. **C,** Venn diagram (top) depicting overlap among ARID1A peaks identified within ChIP-Seq in Bex + Carv–treated sample and the control sample. Venn diagram (bottom) depicting overlap among H3K27ac marks identified within ChIP-Seq in Bex + Carv–treated sample and the control sample. **D,** ChIP-Seq profiles and heat maps of ARID1A and H3K27ac binding, ordered in descending order of ARID1A occupancy. All events clustered into ARID1A lost, constant, or gained binding events upon Bex + Carv treatment compared with the control sample. **E,** Density plots represent the average of ARID1A tags coverage (left 3 plots) in the three different identified clusters, or the average of H3K27ac tags coverage (right 3 plots) associated with ARID1A peaks. ARID1A was immunoprecipitated using 8 µg ARID1A antibody (Santa Cruz Biotechnology, PSG3X/IP). **F,** Enrichment of ARID1A-bound regions in decreased, unchanged, or increased occupancy regions at TRE, FOXM1, and GRHL2 motifs in MCF-7 cells by motif analysis.

ARID1A peak identified in the respective regions were also assessed. In contrast to ARID1A, acetylated H3K27 at the same genomic loci showed a nonsignificant, yet consistently lower level of binding compared with control treatment (**Fig. 3F** and **G**).

The enrichment of ARID1A at the putative regulatory regions of the *IGF-1R* and *IRS1* genes resulted in a decrease in their expression levels upon 48 hours of Bex + Carv treatment in MCF-7 cells. Western blot analysis of IGF-1R and IRS1 proteins showed a moderate, but significant decrease, relative to controls (**Fig. 4A**), while there was no increase in ARID1A protein levels (**Fig. 4B**). Immunostaining in MCF-7 cells confirmed a uniformly distributed, unclustered membrane localization of the IGF-1R, and a cytoplasmic presence of IRS1. Furthermore, quantitative image analysis supported our Western blot findings with a significant reduction in IGF-1R and IRS1 protein levels in Bex + Carv–treated cells (**Fig. 4C** and **D**).
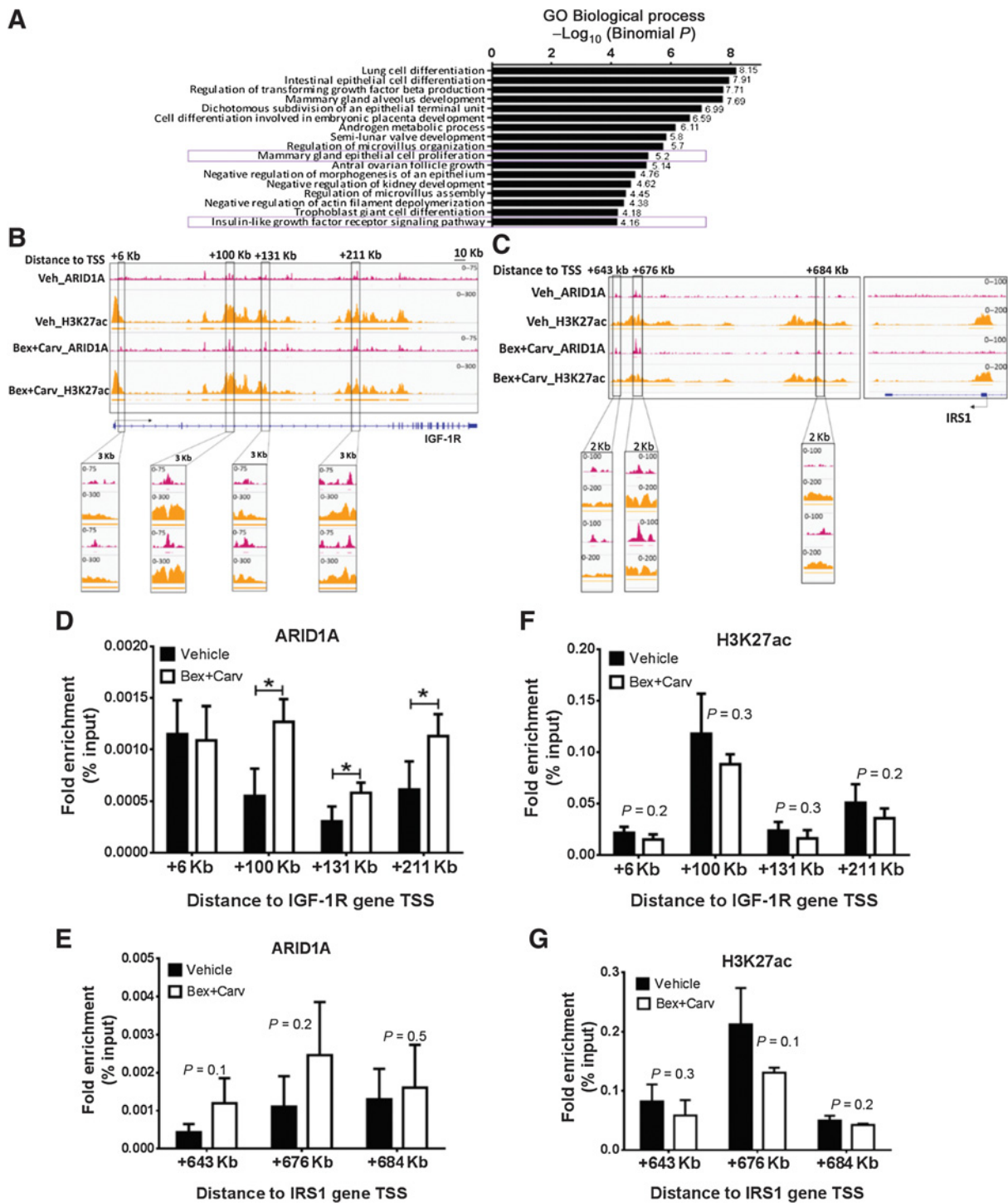
Figure 3.
Functional analysis of ARID1A genomic occupancy in MCF-7 cells upon Bex + Carv treatment. ARID1A and H3K27ac enrichment in genomic loci of the IGF pathway.
A, Gene ontology analysis of the annotated genes related to ARID1A-binding events gained upon Bex + Carv treatment in MCF-7 cells. Integrative Genomics Viewer (IGV) snapshot of ARID1A and H3K27ac ChIP-seq tags coverage representing ARID1A-binding regions related to IGF-1R and IRS1 genes in Bex + Carv or vehicle-treated MCF-7 cells. ChIP-seq tracks of ARID1A and H3K27ac in control and Bex + Carv–treated MCF-7 cells in the genomic locus of IGF-1R (**B**) and IRS1 (**C**) exported from the Integrative Genomics Viewer (IGV) application. **D–G,** Validation for ARID1A enrichment to the target regions of the IGF-1R (**D**) and IRS1 (**E**) genes by ChIP-qPCR in MCF-7 cells. Validation for H3K27ac enrichment to the target regions of the IGF-1R (**F**) and IRS1 genes (**G**) by ChIP-qPCR in MCF-7 cells. $N = 3$ representing three biological replicates. The results are expressed as mean ± SD. *, $P < 0.05$ by two-tailed Student t test.
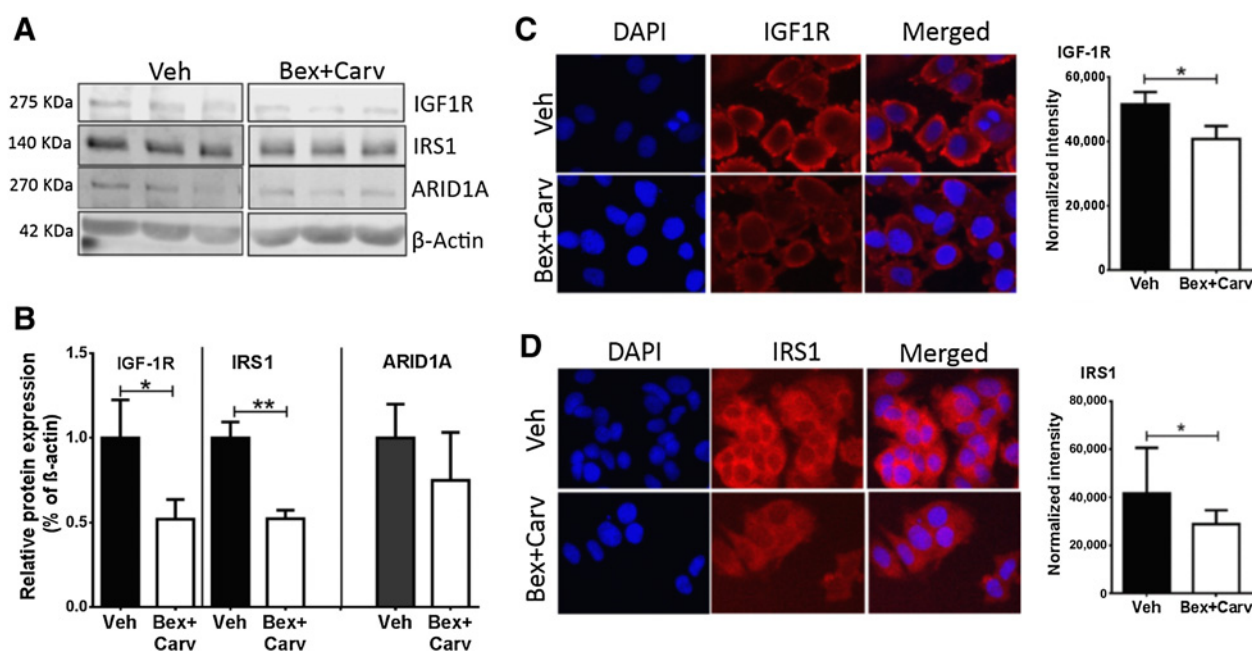
Figure 4.
Determination of IGF-1R and IRS1 protein levels upon Bex + Carv treatment. **A,** Western blot analyses of IGF-1R, IRS1, and ARID1A protein levels in cell extracts from MCF-7 cells treated with vehicle or a combination of Bex and Carv for 48 hours. β-Actin was used as a housekeeping gene. **B,** Quantitation of IGF-1R, IRS1, and ARID1A protein expression upon Bex + Carv treatment in MCF-7 cells. $N = 3$, representing three biological replicates. **C** and **D,** Representative images of MCF-7 cells treated with either vehicle or Bex + Carv for 2 days and immunostained with antibodies against IGF-1R (**C**) or IRS1 (**D**) proteins. DAPI nuclear stain was used to identify the nuclei, 20× magnification. Bar graphs represent the results from quantitative image analysis of at least 200 cells per replicate, based on integrated cellular pixel intensities of the immunostaining for IGF-1R and IRS1 protein expression. The numerical results are expressed as mean ± SD. *, $P < 0.05$; **, $P < 0.01$ by two-tailed Student t test.

To test the impact of ARID1A deficiency on cell growth regulation, gene silencing using a pool of three ARID1A-specific siRNAs was applied, resulting in more than 80% knockdown of both mRNA and protein levels (**Fig. 5A** and **B**). Notably, in subsequent proliferation assays, the suppression of ARID1A was associated with a significant increase in MCF-7 cell counts over a period of 6 days, compared with the control group (**Fig. 5C**). Because knock-down of target genes by siRNAs may affect cells to different degrees, IGF-1R labeling in fluorescent images was evaluated on a cell-by-cell basis. This analysis revealed a marked increase in IGF-1R membrane staining in siARID1A-transfected cells, compared with nontargeting siRNA controls (**Fig. 5D**). However, suppression of ARID1A abrogated the downregulation of IGF-1R upon Bex + Carv treatment (**Fig. 5E**, compare with Fig. 4C). ARID1A knock-down had no effect on the levels of IRS1, but prevented the suppression of IRS1 by Bex + Carv (**Fig. 5F** and **G**). Taken together, these results suggest that ARID1A as a chromatin modulator is essential for the suppression of IGF-1R and IRS1 by Bex + Carv treatment in MCF-7 cells.

Antibodies targeting the IGF-1R have found therapeutic use against various cancers (24, 25). To confirm that the IGF-1 receptor is crucial for maintaining IGF-1 signaling, lastly MCF-7 cells were maintained in the presence or absence of neutralizing anti–IGF-1R antibodies, in normal as well as phenol-red free medium. After a 3-day period, all cells were checked for viability and counted by automated microscopy. No visible loss of viability was observed, but the inhibition of the IGF-1R markedly suppressed cell counts, suggesting a significant role of IGF-1 signal transduction in the proliferation of MCF-7 cells (**Fig. 6A**).

Finally, to determine whether treatments aiming to reduce IGF-1R expression in human breast tumors may carry clinical benefit, RFS was compared in patients with high versus low expression levels of IGF-1R and IRS1. High IGF-1R expression in ER-negative subpopulations was associated with worse outcome (HR, 2.02; $P < 0.001$; classified by both IHC and Affymetrix microarray, **Fig. 6B**). Similar inverse correlation of survival presented itself with high IRS1 expression, selectively in ER-negative cases (**Fig. 6C**).

Discussion

Growth factor signaling pathways often play a central role in cancer cells. IGF-1 promotes survival and proliferation of triple-negative breast cancer cells (26). Mutations in the *IGF-1R* gene are rare and mainly include missense mutations (Supplementary Fig. S1, cBioPortal). However, 2% to 4% of invasive breast carcinomas contain amplifications of the gene as a presumable cause of aberrant IGF-1R expression. Overexpression of IGF-1R has been observed in a number of tumor types, including breast, pancreatic, prostate cancers and sarcomas, accelerating disease progression (27, 28). Upregulation of IGF-1R due to neoadjuvant treatment of breast cancer is associated with poor outcome (29). Moreover, we found that higher transcript levels of IGF-1R or IRS1 in mammary tumors are correlated with increased odds of disease recurrence, selectively in ER-negative breast cancers.

In this study, we show that in MCF-7 breast cancer cells the combination of Bex and Carv causes ARID1A genomic occupancy to be enriched at regulatory regions related to genes of the IGF-1
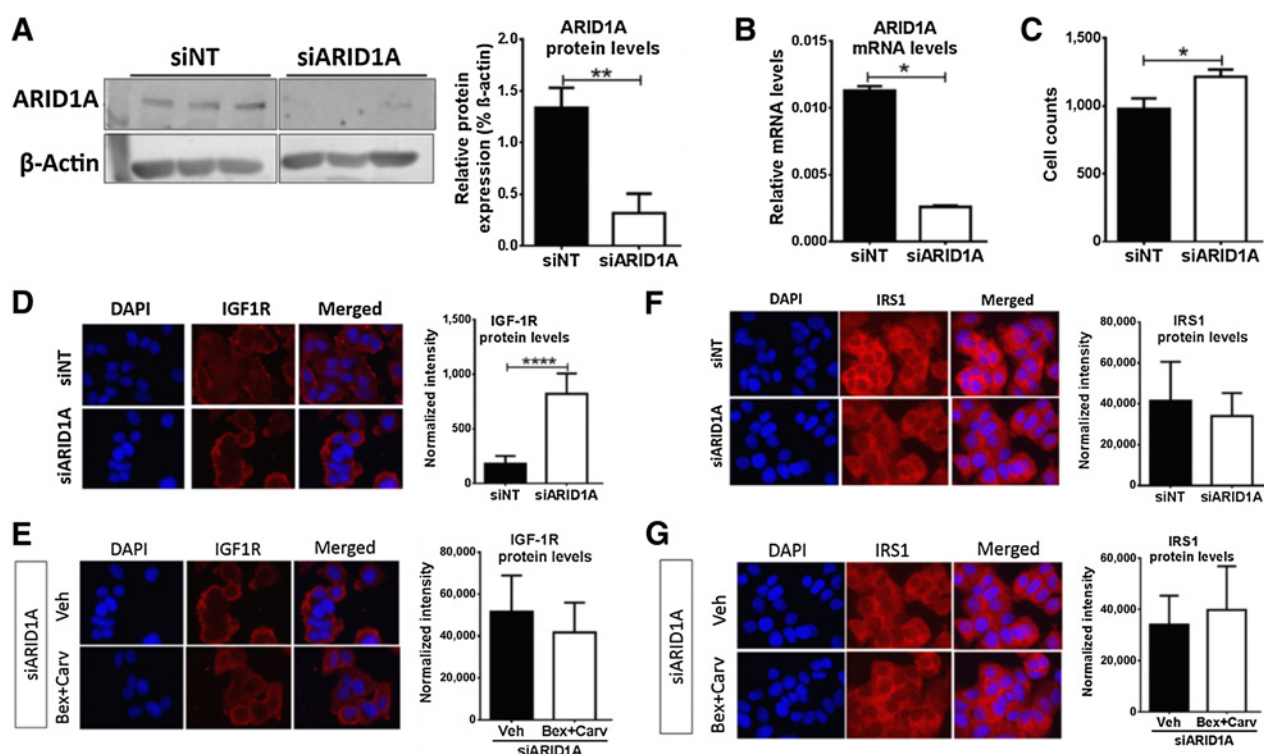
Figure 5.
Knockdown of ARID1A modulates cell proliferation and response to Bex + Carv. **A,** Western blot analysis of cell extracts after nontargeting (siNT) or target-specific (siARID1A) siRNA knock-down of ARID1A. Bar graph, quantitation of ARID1A protein levels in control (siNT) versus ARID1A-specific siRNA-silenced cells. **B,** Comparison of ARID1A mRNA levels in control nontargeting (siNT) and ARID1A-specific siRNA-silenced cells. **C,** Microscopy-based proliferation assay on MCF-7 cells showing cell counts upon ARID1A knock-down 6 days post transfection. Four replicates per treatment were applied and all cells were counted in each well. **D–G,** Image-based analyses of IGF-1R and IRS1 expression in MCF-7 cells after transfection with nontargeting (siNT) or ARID1A-specific siRNA. Protein levels were assessed on the basis of cell-by-cell evaluation of immunostaining from 20× fluorescent microscopy images analyzed by CellProfiler. A minimum of 200 cells per replicate were analyzed. Quantitation of target protein levels in control (siNT) versus ARID1A specific siRNA-transfected cells (**D** and **F**), or ARID1A-silenced cells treated with vehicle or Bex + Carv for 48 hours (**E** and **G**).
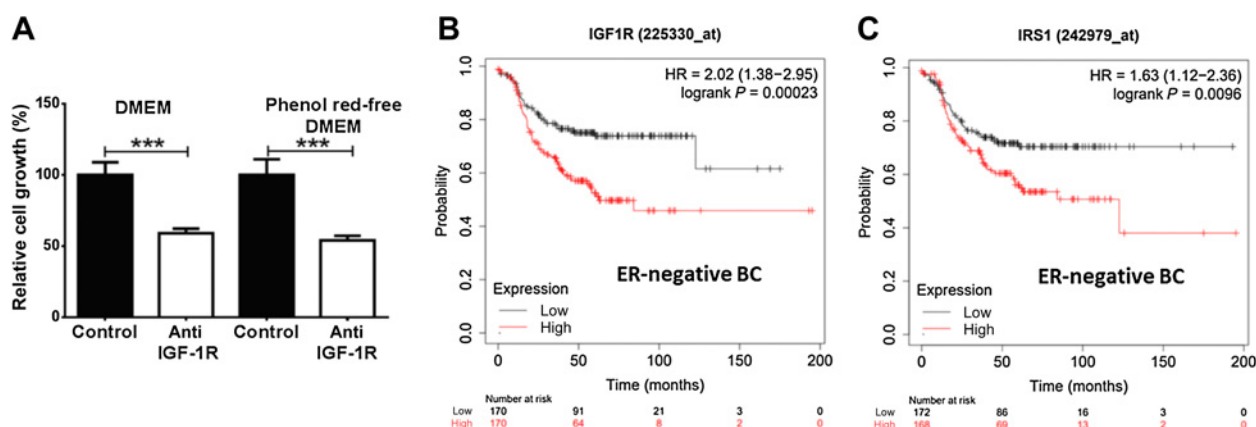

Figure 6.
Assessing the impact of IGF-1R function *in vitro* and *in vivo*. **A,** Image-based measurement of MCF-7 cell proliferation over 3 days in the presence of neutralizing anti–IGF-1R antibody compared with controls, assessed in regular and nonestrogenic (phenol red–free) cell culture media. Results are expressed as mean ± SD. *, $P < 0.05$; **, $P < 0.01$; ***, $P < 0.001$; ****, $P < 0.0001$ by one-way ANOVA, Tukey *post hoc* test. Kaplan–Meier analysis of high versus low IGF-1R mRNA levels (probe 225330_at; **B**) and of high versus low IRS1 mRNA levels (probe 242979_at; **C**) determined by Affymetrix microarrays in ER-negative cases classified using both microarrays and IHC. BC, breast cancer.

pathway including IGF-1R and IRS1. Downregulation of their protein levels upon the combination treatment inhibited MCF-7 cell proliferation more than either drug alone, suggesting a synergistic interaction between Bex and Carv in MCF-7 similar to DCIS cells. Because of the central role of the IGF axis in cell-cycle progression and cell fate determination, functional regulatory regions had been mapped in the past (27, 30). Our ChIP-seq analysis of ARID1A identified new enhancer sites in IGF-1 axis genes not previously studied. Several growth-related genes and transcription factors are known to be regulated by the SWI/SNF complex, but the IGF system may represent a new target for ARID1A.

Although IGF-1R is not considered a main driver of tumor development (31), dysregulation of the IGF pathway has been an attractive therapeutic target for its obvious role in growth signaling (24, 32). In addition, IGF-1–based resistance mechanisms to existing therapies, such as a blunted response to Akt inhibitors in ER-positive breast cancers, necessitate the development of IGF-1–dependent adjuvant strategies (33). Humanized antibodies targeting IGF receptors and small-molecule inhibitors were developed and successfully used in the treatment of soft-tissue sarcoma and Ewing sarcoma (24, 34). Although most clinical trials of IGF-1R–directed monotherapy reported low objective response rates and minor disease stabilization (25), targeting IGF-1R in combinations with other essential drivers of tumor development proved far more promising (35, 36). Inhibitors of ATM-related kinase and CDK4/6 demonstrated synergistic antitumor effects with IGF-1R inhibitors in breast, pancreatic, and other cancer models (37, 38). Ovarian and breast cancers harboring defective homologous recombination capabilities are good targets for the combined inhibition of PARP and the IGF-1R (39). Because a fraction of the cellular IGF-1R pool functions in association with the insulin receptor, direct inhibition of the already formed complexes may fundamentally impact glucose homeostasis, as indicated by adverse events of hyperglycemia (40) (36). In contrast, our data offer a promising novel approach for the control of IGF-1R activity through the modulation of ARID1A.

The transcriptional regulation of IGF-1R is scarcely understood. EGR-1 was shown to exert control over the $5'$ UTR of IGF-1R in prostate cancer cells, and noncoding RNAs play a role in regulating its metabolic impact (30, 41). Interestingly, our motif search also detected binding of ARID1A to EGR-1 motifs in a small fraction of potential genomic targets, yet only upon addition of Bex + Carv (Supplementary Table S2). This suggests that in addition to enhancer sites, ARID1A might regulate IGF-1R expression indirectly through EGR-1 motifs located in the gene promoter. Sarfstein and colleagues previously identified an ER-responsive element in the promoter of the *IGF-1R* gene (42). However, our assay conditions minimized estrogenic impact, while ARID1A was not recruited to the promoter, but to enhancer regions of IGF-1R. Nevertheless, the prospect of the chromatin-level regulation of IGF-1–dependent growth mechanisms in breast cancer cells seems unique to these presented findings. The differential activation of ARID1A upon Bex + Carv in MCF-7 did not occur on the basis of an induction, and thus, is suggested to result from a redistribution, and a significant enrichment of ARID1A at the enhancer sites of *IGF-1R* and *IRS1*.

The SWI/SNF chromatin remodeler complex is involved in the establishment and maintenance of functional chromatin domains. Synthetic lethal strategies targeting the vulnerabilities of SWI/SNF–deficient tumors have been in the forefront of interest due to the high frequency of their occurrence (43, 44). Here we propose a novel perspective, which utilizes intact ARID1A functionality for a therapeutic gain, demonstrating that enhanced ARID1A occupancy tightens the control over IGF-1 signaling and cell growth. ARID1A confers specificity to the SNF/SWI complex and may recruit the complex to its targets in an ATP-dependent manner (45). It is an intriguing question how ARID1A may be involved in transcriptional activation and repression of select genes by chromatin remodeling. According to our model, enhancer sites within the *IGF-1R* and *IRS1* genes are prioritized and enriched by ARID1A binding in the absence of a parallel increase in its expression levels, representing a new example of the transcriptional control exerted by the SWI/SNF complex. The change in IGF-1R and IRS1 protein levels was not correlated with ARID1A expression, suggesting a redistribution of the available ARID1A pool among the SWI/SNF complexes to be the driving factor that regulate IGF-1R and IRS1 expression.

Hormonal status and proliferation are tightly associated due to estrogen and progesterone as mitogens for normal breast epithelium. The role of ARID1A in ER-positive breast cancer cell lineage plasticity and endocrine therapy resistance was elegantly demonstrated using an ARID1A-deficient MCF-7 cell model. ARID1A increased tumor cell sensitivity to ER antagonists by recruiting histone deacetylase (HDAC1) to ER response elements leading to transcriptional suppression of ER target genes (46). Indeed, our motif analysis confirmed the binding potential of ARID1A to EREs, as shown in Supplementary Table S2. To assess the genomic contribution of ARID1A to the rexinoid response, we examined the overall rexinoid-induced genomic occupancy of ARID1A in the well-characterized MCF-7 cell model, without an estrogenic impact. In our model, select promoter regions previously demonstrated to contain ARID1A-dependent ER-binding sites (16) exhibited no change in ARID1A occupancy upon Bex + Carv treatment of MCF-7 cells (Supplementary Fig. S2). In contrast, ARID1A recruitment is prioritized at IGF1-axis regulatory regions when responding to Bex and Carv treatment, leading to the suppression of IGF-1R and IRS1. The transforming activity of oncogenes such as the SV40 T-antigen is affected by the concerted action of both IGF-1R and IRS-1 (47). The coordinated regulation of IGF-1R and IRS1 through the recruitment of ARID1A to distant enhancer regions is in line with these functional ties between IRS1 and IGF-1R.

We also demonstrate that the use of neutralizing antibody to IGF-1R expressed on the surface of MCF-7 cells alone is sufficient to suppress proliferation. A suppressive function of ARID1A in IGF-1R expression is commensurate with this paradigm. In addition to its actions on enhancers of IGF-1–related genes, ARID1A may utilize the binding sites of other hormone-independent transcription factors such as FoxM1 and AP-1, to modulate growth. Recent discoveries of the nuclear import of both subunits of IGF-1R (48) and its recruitment to the promoter of the AP-1 constituent and oncogene JUN raises the possibility of competitive feedback loop between IGF-1R and the SWI/SNF chromatin regulatory complex.

In this study, we found that ARID1A is functionally regulated by the potent antiproliferative combination of Bex and Carv. Bex is currently the only synthetic rexinoid in clinical use with a well-defined, but underutilized chemopreventive and antitumor potential, due to concerns of toxicities occurring at therapeutic dosage (49). Combination therapy has earned much attention due to the ability of reducing the effective doses and thereby side-effects, as well as alleviate resistance mechanisms, in the case of synergistic interactions (50). Combinations of rexinoids with other nuclear receptor ligands have been investigated and proposed in specific tumor types and applications (6–8, 51).

Previous high-throughput combination screens of low-dose Bex in normal and DCIS cells identified the nonselective beta-adrenergic inhibitor, Carv, as a highly effective enhancer of Bex-induced growth suppression. A sufficiently low Bex concentration ensured that the ligand selectively activates the available RXRs, but not RARs (52). The synergy between Bex and Carv is unique, considering the compartmentally different targeting of a nuclear and a cell surface receptor. Despite the many known mechanisms affected, how Bex and Carv specifically inhibit cell proliferation is still unclear. Our findings indicate that the suppression of the IGF-1R and IRS1 genes is directed by ARID1A activity upon Bex + Carv treatment in MCF-7 cells and may play a role in this growth suppression.

The large cluster of several enhancers downstream from the TSS of the *IGF-1R* and the *IRS1* gene confers a concerted action to modulate their expression through a novel enhancer cluster that regulates cell function through the SWI/SNF complex. Epigenetic changes in cancer cells frequently involve super-enhancer units, altering cell phenotype and converting cells to a transcriptional state resistant to chemotherapy (53). The concerted action of Bex + Carv to downregulate IGF-dependent growth in breast cancer cells is commensurate with the pharmacologic profile of rexinoids. However, the contribution of the beta-blocker Carv opens a new intriguing aspect to our current antitumor combination repertoire. Uncovering the full scale of genomic changes may provide further therapeutic opportunities to control cell growth utilizing the SWI/SNF machinery.

References

1. Grinda T, Antoine A, Jacot W, Blaye C, Cottu P-H, Diéras V, et al. Evolution of overall survival and receipt of new therapies by subtype among 20 446 metastatic breast cancer patients in the 2008–2017 ESME cohort. ESMO Open 2021;6: 100114.
2. Garcia-Martinez L, Zhang Y, Nakata Y, Chan HL, Morey L. Epigenetic mechanisms in breast cancer therapy and resistance. Nat Commun 2021;12:1786.
3. Fuqua SA, Wiltschke C, Zhang QX, Borg A, Castles CG, Friedrichs WE, et al. A hypersensitive estrogen receptor-alpha mutation in premalignant breast lesions. Cancer Res 2000;60:4026–9.
4. de Lera AR, Bourguet W, Altucci L, Gronemeyer H. Design of selective nuclear receptor modulators: RAR and RXR as a case study. Nat Rev Drug Discov 2007;6: 811–20.
5. de Almeida NR, Conda-Sheridan M. A review of the molecular design and biological activities of RXR agonists. Med Res Rev 2019;39:1372–97.
6. Liby K, Rendi M, Suh N, Royce DB, Risingsong R, Williams CR, et al. The combination of the rexinoid, LG100268, and a selective estrogen receptor modulator, either arzoxifene or acolbifene, synergizes in the prevention and treatment of mammary tumors in an estrogen receptor-negative model of breast cancer. Clin Cancer Res 2006;12:5902–9.
7. Uray IP, Rodenberg JM, Bissonnette RP, Brown PH, Mancini MA. Cancer-preventive rexinoid modulates neutral lipid contents of mammary epithelial cells through a peroxisome proliferator-activated receptor gamma-dependent mechanism. Mol Pharmacol 2012;81:228–38.
8. Bowen CM, Walter L, Borras E, Wu W, Ozcan Z, Chang K, et al. Combination of sulindac and bexarotene for prevention of intestinal carcinogenesis in familial adenomatous polyposis. Cancer Prev Res 2021;14:851–62.
9. Zhao B, Lin J, Rong L, Wu S, Deng Z, Fatkhutdinov N, et al. ARID1A promotes genomic stability through protecting telomere cohesion. Nat Commun 2019;10: 019–12037.
10. Shen J, Ju Z, Zhao W, Wang L, Peng Y, Ge Z, et al. ARID1A deficiency promotes mutability and potentiates therapeutic antitumor immunity unleashed by immune checkpoint blockade. Nat Med 2018;24:556–62.
11. Cho HD, Lee JE, Jung HY, Oh MH, Lee JH, Jang SH, et al. Loss of tumor suppressor ARID1A protein expression correlates with poor prognosis in patients with primary breast cancer. J Breast Cancer 2015;18:339–46.
12. Ribeiro-Silva C, Vermeulen W, Lans H. SWI/SNF: Complex complexes in genome stability and cancer. DNA Repair 2019;77:87–95.
13. Harrod A, Lane KA, Downs JA. The role of the SWI/SNF chromatin remodelling complex in the response to DNA double strand breaks. DNA Repair 2020;93: 102919.
14. Behbod F, Kittrell FS, Lamarca H, Edwards D, Kerbawy S, Heestand JC, et al. An intraductal human-in-mouse transplantation model mimics the subtypes of ductal carcinoma in situ. Breast Cancer Res 2009;11:R66.
15. Lee AV, Oesterreich S, Davidson NE. MCF-7 cells–changing the course of breast cancer research and care for 45 years. J Natl Cancer Inst 2015;107: djv073.
16. Xu G, Chhangawala S, Cocco E, Razavi P, Cai Y, Otto JE, et al. ARID1A determines luminal identity and therapeutic response in estrogen-receptor-positive breast cancer. Nat Genet 2020;52:198–207.
17. Lin YF, Tseng IJ, Kuo CJ, Lin HY, Chiu IJ, Chiu HW. High-level expression of ARID1A predicts a favourable outcome in triple-negative breast cancer patients receiving paclitaxel-based chemotherapy. J Cell Mol Med 2018; 22:2458–68.
18. Hennessy BT, Lu Y, Gonzalez-Angulo AM, Carey MS, Myhre S, Ju Z, et al. A technical assessment of the utility of reverse phase protein arrays for the study of the functional proteome in non-microdissected human breast cancers. Clin Proteomics 2010;6:129–51.
19. Nagy G, Dániel B, Jónás D, Nagy L, Barta E. A novel method to predict regulatory regions based on histone mark landscapes in macrophages. Immunobiology 2013;218:1416–27.
20. Ashoor H, Hérault A, Kamoun A, Radvanyi F, Bajic VB, Barillot E, et al. HMCan: a method for detecting chromatin modifications in cancer samples using ChIP-seq data. Bioinformatics 2013;29:2979–86.
21. Győrffy B. Survival analysis across the entire transcriptome identifies biomarkers with the highest prognostic power in breast cancer. Comput Struct Biotechnol J 2021;19:4101–9.
22. Wilson MR, Reske JJ, Holladay J, Neupane S, Ngo J, Cuthrell N, et al. ARID1A mutations promote P300-dependent endometrial invasion through super-enhancer hyperacetylation. Cell Rep 2020;33:108366.
23. Lubet RA. Efficacy of Targretin on methylnitrosourea-induced mammary cancers: prevention and therapy dose-response curves and effects on proliferation and apoptosis. Carcinogenesis 2005;26:441–8.
24. Arcaro A. Targeting the insulin-like growth factor-1 receptor in human cancer. Front Pharmacol 2013;4:30.

25. Gradishar WJ, Yardley DA, Layman R, Sparano JA, Chuang E, Northfelt DW, et al. Clinical and translational results of a phase II, randomized trial of an anti-IGF-1R (Cixutumumab) in women with breast cancer that progressed on endocrine therapy. Clin Cancer Res 2016;22:301–9.

26. Davison Z, De Blacquière GE, Westley BR, May FEB. Insulin-like growth factor-dependent proliferation and survival of triple-negative breast cancer cells: implications for therapy. Neoplasia 2011;13:504–15.

27. Nair PN, De Armond DT, Adamo ML, Strodel WE, Freeman JW. Aberrant expression and activation of insulin-like growth factor-1 receptor (IGF-1R) are mediated by an induction of IGF-1R promoter activity and stabilization of IGF-1R mRNA and contributes to growth factor independence and increased survival of the pancreatic cancer cell line MIA PaCa-2. Oncogene 2001;20:8203–14.

28. Jin M, Buck E, Mulvihill MJ. Modulation of insulin-like growth factor-1 receptor and its signaling network for the treatment of cancer: current status and future perspectives. Oncol Rev 2013;7:e3.

29. Heskamp S, Boerman OC, Molkenboer-Kuenen JDM, Wauters CA, Strobbe LJA, Mandigers CMPW, et al. Upregulation of IGF-1R expression during neoadjuvant therapy predicts poor outcome in breast cancer patients. PLoS One 2015;10: e0117745.

30. Chen B, Li J, Chi D, Sahnoune I, Calin S, Girnita L, et al. Non-coding RNAs in IGF-1R signaling regulation: The underlying pathophysiological link between diabetes and cancer. Cells 2019;8:1638.

31. Vogelstein B, Papadopoulos N, Velculescu VE, Zhou S, Diaz LA, Kinzler KW. Cancer genome landscapes. Science 2013;339:1546–58.

32. Rieder S, Michalski CW, Friess H, Kleeff J. Insulin-like growth factor signaling as a therapeutic target in pancreatic cancer. Anticancer Agents Med Chem 2011;11: 427–33.

33. Fox EM, Kuba MG, Miller TW, Davies BR, Arteaga CL. Autocrine IGF-I/insulin receptor axis compensates for inhibition of AKT in ER-positive breast cancer cells with resistance to estrogen deprivation. Breast Cancer Res 2013; 15:R55.

34. Schöffski P, Adkins D, Blay JY, Gil T, Elias AD, Rutkowski P, et al. An open-label, phase 2 study evaluating the efficacy and safety of the anti-IGF-1R antibody cixutumumab in patients with previously treated advanced or metastatic soft-tissue sarcoma or Ewing family of tumours. Eur J Cancer 2013;49:3219–28.

35. Lamhamedi-Cherradi SE, Menegaz BA, Ramamoorthy V, Vishwamitra D, Wang Y, Maywald RL, et al. IGF-1R and mTOR blockade: novel resistance mechanisms and synergistic drug combinations for Ewing sarcoma. J Natl Cancer Inst 2016; 108:djw182.

36. Simpson A, Petnga W, Macaulay VM, Weyer-Czernilofsky U, Bogenrieder T., Insulin-Like Growth Factor (IGF) pathway targeting in cancer: Role of the IGF axis and opportunities for future combination studies. Target Oncol 2017;12: 571–97.

37. O'flanagan CH, O'shea S, Lyons A, Fogarty FM, Mccabe N, Kennedy RD, et al. IGF-1R inhibition sensitizes breast cancer cells to ATM-related kinase (ATR) inhibitor and cisplatin. Oncotarget 2016;7:56826–41.

38. Miller ML, Molinelli EJ, Nair JS, Sheikh T, Samy R, Jing X, et al. Drug synergy screen and network modeling in dedifferentiated liposarcoma identifies CDK4 and IGF1R as synergistic drug targets. Sci Signal 2013;6:ra85.

39. Amin O, Beauchamp MC, Nader PA, Laskov I, Iqbal S, Philip CA, et al. Suppression of homologous recombination by insulin-like growth factor-1 inhibition sensitizes cancer cells to PARP inhibitors. BMC Cancer 2015;15: 817.

40. Ma H, Zhang T, Shen H, Cao H, Du J. The adverse events profile of anti-IGF-1R monoclonal antibodies in cancer therapy. Br J Clin Pharmacol 2014;77:917–28.

41. Ma Y, Cheng Q, Ren Z, Xu L, Zhao Y, Sun J, et al. Induction of IGF-1R expression by EGR-1 facilitates the growth of prostate cancer cells. Cancer Lett 2012;317: 150–6.

42. Sarfstein R, Belfiore A, Werner H. Identification of Insulin-Like Growth Factor-I Receptor (IGF-IR) gene promoter-binding proteins in Estrogen Receptor (ER)-positive and ER-depleted breast cancer cells. Cancers 2010;2:233–61.

43. Shen J, Peng Y, Wei L, Zhang W, Yang L, Lan L, et al. ARID1A deficiency impairs the DNA damage checkpoint and sensitizes cells to PARP inhibitors. Cancer Discov 2015;5:752–67.

44. Sasaki M, Ogiwara H. Synthetic lethal therapy based on targeting the vulnerability of SWI/SNF chromatin remodeling complex-deficient cancers. Cancer Sci 2020;111:774–82.

45. Wilsker D. The DNA-binding properties of the ARID-containing subunits of yeast and mammalian SWI/SNF complexes. Nucleic Acids Res 2004;32:1345–53.

46. Nagarajan S, Rao SV, Sutton J, Cheeseman D, Dunn S, Papachristou EK, et al. ARID1A influences HDAC1/BRD4 activity, intrinsic proliferative capacity and breast cancer treatment response. Nat Genet 2020;52:187–97.

47. Deangelis T, Chen J, Wu A, Prisco M, Baserga R. Transformation by the simian virus 40 T antigen is regulated by IGF-I receptor and IRS-1 signaling. Oncogene 2006;25:32–42.

48. Mills JV, Osher E, Rieunier G, Mills IG, Macaulay VM. IGF-1R nuclear import and recruitment to chromatin involves both alpha and beta subunits. Discov Oncol 2021;12:13.

49. Uray IP, Dmitrovsky E, Brown PH. Retinoids and rexinoids in cancer prevention: from laboratory to clinic. Semin Oncol 2016;43:49–64.

50. Meyer CT, Wooten DJ, Paudel BB, Bauer J, Hardeman KN, Westover D, et al. Quantifying drug combination synergy along potency and efficacy axes. Cell Syst 2019;8:97–108.

51. Brown PH, Subbaramaiah K, Salmon AP, Baker R, Newman RA, Yang P, et al. Combination chemoprevention of HER2/neu-induced breast cancer using a cyclooxygenase-2 inhibitor and a retinoid X receptor-selective retinoid. Cancer Prev Res 2008;1:208–14.

52. Jurutka PW, Wagner CE. Methods to assess activity and potency of rexinoids using rapid luciferase-based assays: a case study with NEt-TMN. Methods Mol Biol 2019;2019:95–108.

53. Shaffer SM, Dunagin MC, Torborg SR, Torre EA, Emert B, Krepler C, et al. Rare cell variability and drug-induced reprogramming as a mode of cancer drug resistance. Nature 2017;546:431–5.